

Reconfinement of highly magnetized jets: Implications for HST-1 in M87

A. Levinson,^{1*} N. Globus,²

¹Raymond and Beverly Sackler School of Physics & Astronomy, Tel Aviv University, Tel Aviv 69978, Israel

²Racah Institute of Physics, The Hebrew University of Jerusalem, 91904 Jerusalem, Israel

Released 9 March 2022

ABSTRACT

Stationary features are occasionally observed in AGN jets. A notable example is the HST-1 knot in M87. Such features are commonly interpreted as re-confinement shocks in hydrodynamic jets or focusing nozzles in Poynting jets. In this paper we compute the structure and Lorentz factor of a highly magnetized jet confined by external pressure having a profile that flattens abruptly at some radius. We find the development of strong oscillations upon transition from the steeper to the flatter pressure profile medium. Analytic formula is derived for the location of the nodes of these oscillations. We apply the model to the M87 jet and show that if the jet remains magnetically dominated up to sub-kpc scales, then focusing is expected. The location of the HST-1 knot can be reconciled with recent measurements of the pressure profile around the Bondi radius if the jet luminosity satisfies $L_j \simeq 10^{43}$ erg/s. However, we find that magnetic domination at the collimation break implies a Lorentz factor in excess of 10^2 , atypical to FRI sources. A much lower value of the asymptotic Lorentz factor would require substantial loading close to the black hole. In that case HST-1 may be associated with a collimation nozzle of a hydrodynamic flow.

Key words: . galaxies: active - galaxies: jets - shock waves - ISM: jets and outflows

1 INTRODUCTION

HST-1 is a stationary radio feature associated with the sub-kpc scale jet in M87 (Biretta et al. 1999). The knot is located at a projected distance of 60 pc (0.86'') from the central engine, and is known to be a region of violent activity. Subfeatures moving away from the main knot of the HST-1 complex at superluminal speeds have been detected (Biretta et al. 1999; Cheung et al. 2007, Giroletti et al. 2012), indicating that a highly relativistic flow is passing through this region. Moreover, the reported variability of the resolved X-ray and optical emission from HST-1 implies that the (beaming corrected) size of the emission region is much smaller than the distance between the HST-1 knot and the central black hole (e.g., Cheung et al. 2007), suggesting a strong focusing of the flow at this location. Stationary radio features, similar to HST-1, are quite common in radio loud AGNs (e.g., Coehn, et al. 2014) and may have the same origin.

It has been proposed that the stationary knot in the HST-1 complex is associated with a recollimation shock that forms either, due to a change in the gradient of the external pressure (Stawarz et al. 2006; Bromberg & Levinson 2009, hereafter ST06 and BL09), or by hoop stresses of a subrelativistic, magnetized wind surrounding the spine, as in the two-component MHD model of Garcia et

al. (2009; see also Nakamura et al. 2010). The recollimation shock scenario is further supported by the sudden change in the collimation profile observed at the location of HST-1 (Nakamura & Asada 2013). In this picture, the rapid variability of the HST-1 emission and the ejection of superluminal subknots from the HST-1 complex are associated with internal shocks produced by self-reflection of the converging flow at the axis, just downstream of the recollimation nozzle (Bogovalov & Tsinganos 2005; Levinson & Bromberg 2008; Nakamura et al. 2010, 2014).

A question of interest is whether the M87 jet is highly or weakly magnetized at the recollimation nozzle. ST06 considered a hydrodynamic jet, and proposed that HST-1 reflects the location at which the reconfinement shock reaches the jet axis. They did not attempt to reproduce the entire collimation profile, but merely to demonstrate that convergence of the shock occurs under the conditions inferred from observations. BL09 have shown that strong focusing of a hydrodynamic jet at the reflection point is anticipated if the plasma behind the oblique shock cools rapidly. Both, ST06 and BL09 attribute the location of the nozzle to a change in the external pressure profile. In the two-component MHD model (Bogovalov & Tsinganos 2005, Garcia et al. 2009), on the other hand, the focusing of the jet is not related to the properties of the ambient medium, but rather to the dynamics of a magnetized spine-sheath structure. This model can reproduce the entire collimation profile upon appropriate choice of model parameters. However, it requires

* E-mail: levinson@wise.tau.ac.il

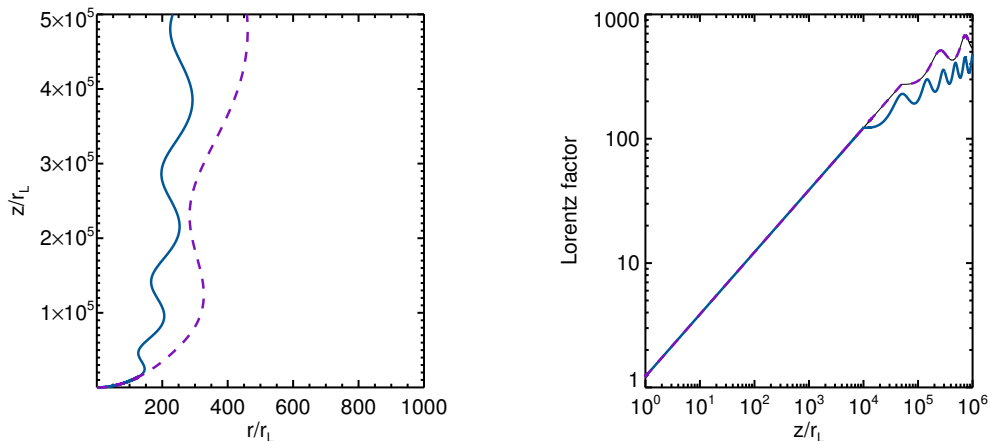


Figure 1. Jet profile (lef panel) and Lorentz factor (right panel) computed using a confining pressure of the form $\mathcal{P}_{ext} = A z^{-2}$ at $z < z_{tr}$ and $\mathcal{P}_{ext} = (A/z_{tr}) z^{-1}$ at $z > z_{tr}$, for $z_{tr} = 10^4$ (solid line) and $z_{tr} = 5 \times 10^4$ (dashed line).

the existence of an extended MHD disk wind with a regular magnetic field which, in our view, is highly questionable. The observed collimation profile within the Bondi radius can also be reproduced if the inner, Poynting jet, is confined by a hydrodynamic (weakly magnetized) disk wind (Globus & Levinson 2016, hereafter GL16). Whether it can also account for the change in structure across the Bondi radius is one of the issues addressed in this paper.

A highly magnetized jet is expected to undergo strong oscillations when encountering a medium with a flat pressure profile, $p_{ext}(z) \propto z^{-\kappa}$, $\kappa < 2$ (Lyubarsky 2009, Komissarov et al. 2015, Mizuno et al. 2015). These oscillations occur in cases where the jet is not in its equilibrium state when encountering the confining medium (Lyubarsky 2009), and can be ascribed to a standing magnetosonic wave. In reality, substantial focusing of the jet should lead to a rapid growth of current-driven internal kink modes, and the subsequent dissipation of the magnetic field (Bromberg & Tchekhovskoy 2016, Singh et al. 2016). Thus, focusing of a Poynting jet can, in principle, produce stationary jet features with observational imprints similar to those observed in M87 and other AGNs.

In this paper we address the following question: can HST-1 in M87 be produced by the focusing of a Poynting-flux dominated jet in a way that satisfies all observational constraints? And if so, what are the implications for jet dynamics?

2 MODEL DESCRIPTION AND RESULTS

In the following, we use cylindrical coordinates (r, ϕ, z) , with the z axis aligned with the jet symmetry axis. We seek to compute the profile and Lorentz factor of a strongly magnetized jet confined by external pressure, $p_{ext}(z)$, with a changing profile. To be concrete, we suppose that the gradient of the external pressure changes abruptly across a transition point, henceforth denoted by z_{tr} , from a steeper profile, $p_{ext}(z) = p_{<}(z)$ at $z < z_{tr}$, to a flatter profile, $p_{ext}(z) = p_{>}(z)$ at $z > z_{tr}$. In what follows, we normalize the ex-

ternal pressure to the fiducial value

$$p_0 = \frac{2L_j}{3\pi c r_L^2} = 200 L_{j44} (r_L/r_s)^{-2} \left(\frac{M_{BH}}{6 \times 10^9 M_\odot} \right)^{-2} \text{ dyn cm}^{-2}, \quad (1)$$

where $L_j = 10^{44} L_{j44}$ erg/s is the total jet power, $r_L = c/\Omega$ is the radius of the light cylinder, and $r_s = 1.8 \times 10^{15} (M_{BH}/6 \times 10^9 M_\odot)$ cm is the Schwarzschild radius, and denote $\mathcal{P}_{ext}(z) = p_{ext}(z)/p_0$. The shape of the jet radius, $r_j(z)$, is computed by employing the asymptotic transfield equation derived in Lyubarsky (2009), which holds well above the light cylinder in regions where the jet is confined. Upon substituting $L_j = (B_0^2/4\pi)c\pi r_L^2$, where B_0 is the strength of the magnetic field at r_L , and using Equation (1), it reads:

$$\frac{d^2 r_j(z)}{dz^2} = \frac{1}{[r_j(z)]^3} - \mathcal{P}_{ext}(z) r_j(z). \quad (2)$$

Henceforth all lengths are measured in units of r_L unless otherwise specified. The corresponding Lorentz factor at the jet boundary is given by (Lyubarsky 2009)

$$\Gamma(z) = 3^{1/4} \mathcal{P}_{ext}^{-1/2} r_j^{-1}. \quad (3)$$

It is worth noting that in general the Lorentz factor is not uniform across the jet. It increases from its minimum value on the jet axis to its maximum value near the boundary (Lyubarsky 2009).

Equation (2) is integrated numerically using the prescribed pressure $\mathcal{P}_{ext}(z)$. For illustration we consider a pressure profile of the form $\mathcal{P}_{ext} = A z^{-2}$ at $z < z_{tr}$ and $\mathcal{P}_{ext} = B z^{-\kappa}$, $\kappa < 2$, at $z > z_{tr}$, with $B = A z_{tr}^{\kappa-2}$. As discussed in Lyubarsky (2009), for the former profile solutions with $A < 1/4$ correspond to non-equilibrium collimation, whereas $A > 1/4$ corresponds to an intermediate case. For the intermediate case ($A > 1/4$) we choose the initial values of our integration, at $z = 1$, to reproduce the non-oscillatory analytic solution derived in Lyubarsky (2009), $r_j = z^{1/2}/(A - 1/4)^{1/4}$, in the region $z < z_{tr}$. In the non-equilibrium regime ($A < 1/4$), the solution in the region $z < z_{tr}$ always approaches $r_j \propto z^\eta$, $\eta = (1 + \sqrt{1 - 4A})/2$, at sufficiently large z (Komissarov et al. 2009; Lyubarsky 2009). In this regime our initial conditions are simply $r_j(z = 1) = r_{j0}$, $dr_j/dz|_{z=1} = \eta r_{j0}$. We then integrate Equation (2) from $z = 1$ across the transition point to $z \gg z_{tr}$, using the appropriate pressure profile in each region.

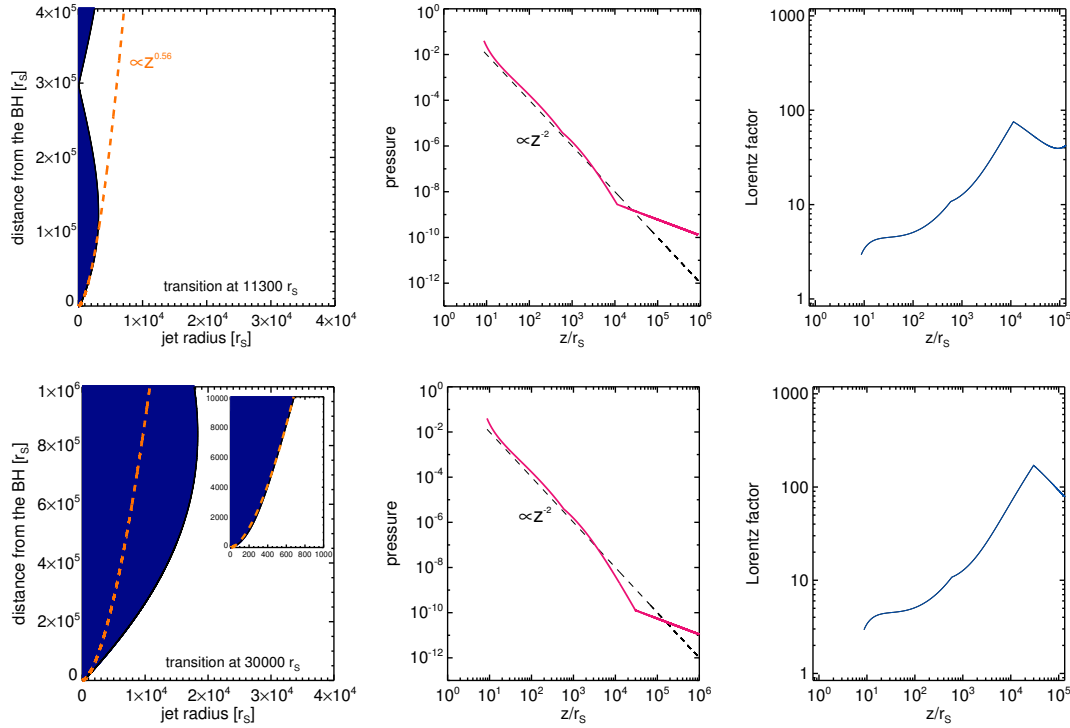


Figure 2. Profiles of jet radius (left panels), pressure (middle panels) and Lorentz factor (right panels) for the M87 jet model. The upper panels correspond to a transition radius of $z_{tr} = 1.1 \times 10^4 r_s$ and the bottom panels to $z_{tr} = 3 \times 10^4 r_s$. In the left panels the vertical axis marks the distance to the black hole, and the horizontal axis the jet radius. The pressure is normalized to the fiducial value given in Equation (1). The dashed red line in the left panels marks the profile $r_j \propto z^{0.58}$ observed below the collimation break (Nakamura & Asada 2013). The inset in the lower left panel is a zoom-in of the inner jet region, presented here for clarity.

An example is shown in Figure 1 for $\kappa = 1$ and two different values of the transition point; $z_{tr} = 10^4$ (solid line) and $z_{tr} = 5 \times 10^4$ (dashed line). As seen, the jet undergoes strong oscillations upon encountering the flat pressure profile medium at $z > z_{tr}$. The amplitude of these oscillations increases with decreasing pressure at the transition point (see appendix). The wavelength of the oscillations depend on the pressure at the transition point, $\mathcal{P}_{ext}(z_{tr})$, and the slope κ . The derivation in the appendix yields an estimate for the location of the nodes:

$$z_n = \left[\frac{(n + 1/2 + \alpha - n\kappa/2 - \alpha\kappa/2 - \kappa/8)\pi}{z_{tr} \sqrt{\mathcal{P}_{ext}(z_{tr})}} \right]^{1/(1-\kappa/2)} z_{tr}, \quad n = 0, 1, 2, \dots, \quad (4)$$

restricted to $z_n > z_{tr}$, where α is a real number between 0.5 and 1, that depends on the phase of the solution at $z = z_{tr}$. At low pressures, viz., $z_{tr} \sqrt{\mathcal{P}_{ext}(z_{tr})} \ll 1$, α approaches either 0.5 or 1 (see appendix). Equation (4) is in excellent agreement with our numerical results. As noted above, in reality rapid dissipation of the magnetic field is expected at the first focusing point, that may alter the subsequent evolution of the jet. By employing Equations (1) and (4) and the relation $\mathcal{P}_{ext}(z_{tr})(z_{tr}/z_0)^\kappa = \mathcal{P}_{ext}(z_0)$, and adopting $\alpha = 1/2$, we obtain the pressure at the first focusing point ($n = 0$):

$$p_{ext}(z_0) = 7 \times 10^{-8} (1 - 3\kappa/8)^2 L_{j44} \left(\frac{z_0}{100 \text{ pc}} \right)^{-2} \text{ dyn cm}^{-2}, \quad (5)$$

independent of the black hole mass.

2.1 Application to M87

We now apply the model outlined above to the HST-1 knot in M87. This stationary feature, located at a projected distance of about 60 pc from the core, appears to be associated with a change in the collimation profile of the jet (Nakamura & Asada 2013), as anticipated in a collimation nozzle. The apparent speed of superluminal motions on kpc scales constraint the viewing angle to the M87 jet to be less than about 20° . Below we adopt a viewing angle of 18° , that yields an actual distance of 200 pc for HST-1, or $3 \times 10^5 r_s$ for a black hole mass of $M_{BH} = 6 \times 10^9 M_\odot$. The collimation profile of the jet has been probed down to about $10 r_s$. It maintains a parabolic shape ($r_j \propto z^{0.58}$) all the way up to the transition point, above which it becomes roughly conical. This readily implies that the profile of the confining pressure in this region is roughly $p_{ext} \propto z^{-2}$. As shown elsewhere (GL16), the collimation profile of the jet below the transition point can be reproduced through a collision of a disk wind with the jet, for a certain choice of jet-to-wind power ratio. In this model the confining pressure in Equation (2) is obtained self-consistently from the compression of the disk wind near the jet boundary. Although the origin of the confining pressure is not important for the present analysis, as a matter of convenience we use the method outlined in GL16 to integrate Equation (2) below the transition point.

Above the transition point we invoke an external pressure of the form $p_>(z) = p_{tr}(z/z_{tr})^{-\kappa}$, with $\kappa \approx 0.7$ and p_{tr} determined by the requirement that the pressure is continuous across the transition. This profile is inferred from X-ray observations on scales 0.2 – 10 kpc (Russell et al. 2015), with a normalization $p(z = 100 \text{ pc}) = 10^{-9}$

dyn cm⁻². We suppose that this profile extends down to z_{tr} . In the following calculations, we adopt the value $r_L = 2.25 r_s$ obtained in Globus & Levinson (2014) for the outer light surface of an equatorial, force-free outflow from a Kerr black hole with a spin parameter $a = 0.9$, assuming a rigid rotation of magnetic field lines with angular velocity $\Omega = \Omega_H/2$, where Ω_H is the angular velocity of the black hole.

Figure 2 shows the resultant jet radius, pressure profile and Lorentz factor, for $z_{tr} = 1.1 \times 10^4 r_s$ and $z_{tr} = 3 \times 10^4 r_s$. As can be seen, the location of the first focusing point is in good agreement with Equation (4) upon substituting $\alpha = 0.5$ and the value of $\mathcal{P}(z_{tr})$ obtained from our integration (middle panels). Note that z and r_j in Figure 2 are measured in units of r_s , not r_L . The value of z_{tr} in the solution presented in the upper panels was chosen such that it reproduces the observed structure. The solution in the lower panels is exhibited for comparison. Both solutions are essentially the same up to the transition radius roughly. We find, quite generally, that the location of the focusing point can be reconciled with the observed collimation break of the M87 jet provided $z_{tr} \approx 10$ pc and $\mathcal{P}(z_{tr}) \approx 1.8 \times 10^{-9}$ (see upper left panel), or using Equation (1) $p_{ext}(z_{tr}) = 7 \times 10^{-8} L_{j44}$ dyn cm⁻², independent of the black hole mass. This value is consistent with the ambient pressure inferred from X-ray observations (Russell et al. 2015) provided

$$L_{j44} = \left[\frac{p_{obs}(z = 100 \text{ pc})}{7 \times 10^{-8} \text{ dyn cm}^{-2}} \right] \left(\frac{z_{tr}}{100 \text{ pc}} \right)^{-0.7} \approx 0.07. \quad (6)$$

The Lorentz factor exhibited in the right panels of figure 2 was computed for a magnetically dominated jet. As seen, the observed collimation profile of the M87 jet implies that a Poynting dominated jet should accelerate to a Lorentz in excess of 10^2 at the focusing nozzle. This value is much higher than the average value inferred from statistics of superluminal motions (e.g., Kellermann et al. 2007). Either the M87 jet is unique, or loading close to the black hole limits the terminal Lorentz factor. For example, $\Gamma_j = 10$ is achieved at a distance of about $200 r_s$ from the putative black hole. We note that the collimation profile is expected to be insensitive to the local magnetization parameter, but the properties of the collimation nozzle may depend on it. If saturation occurs well below the collimation break, then HST-1 may reflect an MHD (Nakamura et al. 2010) or a hydrodynamic (ST06, BL09) shock.

Recent kinematic measurements on scales $100 - 5000 r_s$ reveal substantial stratification of the flow, with a range of Lorentz factors $\Gamma \sim 1 - 3$ (Asada et al. 2014; Mertens et al. 2016). These values are somewhat lower than the Lorentz factor exhibited in the upper right panel of figure 2. However, one should keep in mind that the profile shown in figure 2 corresponds to the Lorentz factor at the jet boundary. In general the Lorentz factor vary across the jet, and has lower values away from the boundary (see comment below Equation 3), so one must be cautious in interpreting observational results. Moreover, it could be that the emission observed on those scales originates from a slower sheath flow (e.g., Moscibrodzka et al. 2016; GL16), as seems to be indicated by the detection of subluminal motions in this region.

3 SUMMARY AND CONCLUSIONS

A Poynting-flux dominated jet undergoes strong focusing upon encountering a confining medium with a flat pressure profile, $p_{ext} \propto z^{-\kappa}$, $\kappa < 2$. At the focusing nozzle, rapid growth of internal kink modes, followed by dissipation of the magnetic field is anticipated (Bromberg & Tchekhovskoy 2016, Singh et al. 2016). This can lead

to the appearance of stationary emission features, as occasionally seen in radio loud AGNs.

In case of M87 we find that the entire collimation profile can be reproduced if the confining pressure profile changes from approximately $p_{ext} \propto z^{-2}$ to the profile observed on scales 0.1-10 kpc, $p_{ext} \propto z^{-0.7}$. The location of the HST-1 knot can be reconciled with the measured pressure provided that the jet power on those scales is $L_j \approx 10^{43}$ erg/s. This value is significantly lower than the power of the large scale jet estimated from various observations (Bicknell & Begelman 1996; de Gasperin et al. 2012), but is consistent with values obtained in recent GRMHD simulations (Moscibrodzka et al. 2016). As pointed out in the later reference, the jet power may be intermittent on timescales much shorter than the age of the system, roughly 30 Myr, and so it is conceivable that it is currently in a low state, well below the average power estimated on large scales. It is also found that if the jet remains magnetically dominated up to the focusing nozzle, here associated with the stationary feature in the HST-1 complex, then its Lorentz factor should be in excess of several hundreds. Such a high Lorentz factor is atypical to FRI sources, as inferred from statistics of superluminal motions (e.g., Kellermann et al. 2007). A much lower value of the asymptotic Lorentz factor would require substantial loading close to the black hole. We do not expect significant alteration of the collimation profile of the loaded jet, but the nature of HST-1 may be different.

The relative proximity of HST-1 to the black hole implies that the confining pressure around the Bondi radius, that produces the collimation break, is unlikely to be supported by the cocoon produced by the relativistic jet, as hinted by Tchekhovskoy & Bromberg (2016). Whether the interaction of disk winds with the ambient medium can account for the observed pressure profile on those scales remains to be investigated. If the jet is indeed collimated by disk winds, as proposed recently (GL16), then one naively anticipates strong shocks to form by virtue of the interaction of the disk wind with the flat density galaxy core.

We thank Masanori Nakamura for enlightening discussions and useful comments. AL acknowledges the support of The Israel Science Foundation (grant 1277/13). NG acknowledges the support of the I-CORE Program of the Planning and Budgeting Committee and The Israel Science Foundation (grant 1829/12) and the Israel Space Agency (grant 3-10417).

APPENDIX A: ANALYSIS OF JET OSCILLATIONS

For the external pressure invoked in the region $z > z_{tr}$ in section 2, $\mathcal{P}_{ext}(z) = Bz^{-\kappa}$, $\kappa < 2$, the transfield equation admits the analytic solution (Lyubarsky 2009)

$$r_j = \sqrt{\frac{2-\kappa}{\pi}} \left(\frac{z^{\kappa}}{B} \right)^{1/4} \Phi(z) \quad (A1)$$

here

$$\Phi(z) = \frac{1}{C_1} \cos^2 S + C_1 \left(C_2 \cos S + \frac{\pi}{2-\kappa} \sin S \right)^2, \quad (A2)$$

and

$$S = \frac{2\sqrt{B}}{2-\kappa} z^{1-\kappa/2} - \frac{(4-\kappa)\pi}{(2-\kappa)4}. \quad (A3)$$

This solution needs to be matched to the solution invoked in section 2 in the region $z < z_{tr}$. The coefficients C_1 and C_2 are then determined from the requirement that $r_j(z)$ and its derivative are continuous at the transition point z_{tr} . For $z_{tr} \gg 1$ the minima of $r_j(z)$ coin-

side to a good approximation with the minima of the function $\Phi(z)$. The minima of Φ occur at the phases $\varphi_n = (\alpha + n)\pi$, $n = 0, 1, 2, \dots$, with $1/2 < \alpha < 1$, given by

$$\cos \varphi_n = \frac{(-1)^{n+1}}{1 + (b + \sqrt{b^2 + 1})^2} \quad (\text{A4})$$

in terms of

$$b = \frac{2 - \kappa}{2\pi C_1^2 C_2} + \frac{(2 - \kappa)C_2}{2\pi} - \frac{\pi}{2(2 - \kappa)C_2}. \quad (\text{A5})$$

The location of the nodes is determined from the relation $S(z_n) = \varphi_n$. In the limit $|b| \gg 1$ one finds $\cos \varphi_n \rightarrow 0$ for $b > 0$, corresponding to $\alpha = 1/2$, and $\cos \varphi_n \rightarrow (-1)^{n+1}$ for $b < 0$, corresponding to $\alpha = 1$.

REFERENCES

- Asada K., Nakamura M., Doi A., Nagai H., Inoue M., 2014, *ApJ*, 781, L2
- Bicknell, G. V., & Begelman, M. C. 1996, *ApJ*, 467, 597
- Biretta, J. A., Sparks, W. B., & Macchetto, F. 1999, *ApJ*, 520, 621
- Bogovalov, S., & Tsinganos, K. 2005, *MNRAS*, 357, 918
- Bromberg, O. & Levinson, A. 2009, *ApJ*, 699, 1274
- Bromberg O. & Tchekhovskoy, A. 2016, *MNRAS*, 456, 1739
- Cheung, C. C., Harris, D. E., & Stawarz, L. 2007, *ApJ*, 663, L65
- Cohen M. H., Meier, D. L., Arshakian T. G., Homan, D. C., Hovatta, T., Kovalev, Y. Y., Lister, M. L., Pushkarev, A. B., Richards, J. L., Savolainen T. 2014, *ApJ*, 787, 151
- de Gasperin F., et al., 2012, *A&A*, 547, A56
- Gracia, J.; Vlahakis, N.; Agudo, I.; Tsinganos, K.; Bogovalov, S. V. 2009, *ApJ*, 695, 503
- Giroletti, M. et al. 2012, *A&A*, 538, 10
- Globus, N.; Levinson, A. 2016, *MNRAS*, 461, 2605
- Kellermann, K. I. et al. 2007, *A&SS*, 311, 231
- Komissarov S., Vlahakis N., Konigl A., Barkov M. V., 2009, *MNRAS*, 394, 1182
- Komissarov, S. S.; Porth, O.; Lyutikov, M. 2015, *ComAC*, 2, 9
- Levinson A. & Bromberg, O. 2008, *IJMPD*, 17, 1603
- Lyubarsky, Y. 2009, *ApJ*, 698, 1570
- Mertens F., Lobanov A. P., Walker R. C., Hardee P. E., 2016, *arXiv*, arXiv:1608.05063
- Mizuno, Y., Gomez, J. L., Nishikawa, K.-I., Meli, A., Hardee, P. E., and Rezzolla, L. 2015, *ApJ*, 809, 28
- Mościbrodzka M., Falcke H., Shiokawa H., 2016, *A&A*, 586, A38
- Nakamura, M., Garofalo, D. & Meier, D. L., 2010, *ApJ*, 721, 1783
- Nakamura M., Asada K., 2013, *ApJ*, 775, 118
- Nakamura, M. & Meier, D. L. 2014, *ApJ*, 785, 152
- Russell, H. R., Fabian, A. C., McNamara, B. R., Broderick, A. E. 2015, *MNRAS*, 451, 588
- Singh, Chandra B.; Mizuno, Yosuke; de Gouveia Dal Pino, Elisabete M. 2016, *ApJ*, 824, 48
- Stawarz, L., Aharonian, F., Kataoka, J., et al. 2006, *MNRAS*, 370, 981
- Tchekhovskoy A., Bromberg O., 2016, *MNRAS*, 461, L46